Petrogenesis of Late Jurassic Qianlishan granites and mafic dykes, Southeast China: implications for a back-arc extension setting

YAO-HUI JIANG*, SHAO-YONG JIANG, KUI-DONG ZHAO & HONG-FEI LING

State Key Laboratory for Mineral Deposits Research, Department of Earth Sciences, Nanjing University,
Nanjing 210093, P.R. China

Abstract – A late Mesozoic belt of volcanic-intrusive complexes occurs in Southeast China. The Qianlishan granites are distributed in the northwest of the belt. The pluton is composed of porphyritic biotite granite (153 Ma) and equigranular biotite granite (151 Ma) and was intruded by granite-porphyry dykes (144 Ma) and mafic dykes such as lamprophyre and diabase (142 Ma). The granitic rocks, consisting mainly of K-feldspar, plagioclase, quartz and Fe-rich biotite, have SiO_2 contents of 72.9–76.9 %, and are enriched in alkalis, rare earth elements (REE), high field strength elements (HFSE) and Ga with high Ga/Al ratios, but depleted in Ba, Sr and transition metals. Trace-element geochemistry and Sr–Nd isotope systematics further imply that the Qianlishan granitic magmas were most probably derived by partial melting of Palaeo- to Mesoproterozoic metamorphic lower-crustal rocks that had been granulitized during an earlier thermal event. These features suggest an A-type affinity. The Qianlishan lamprophyre and neighbouring coeval mafic dykes ($SiO_2 = 47.9$–53.8 wt %) have high MgO and compatible element contents. These rocks also have high K_2O contents and are enriched in alkalis, light REE, large ion lithophile elements, and depleted in HFSE. They have low initial ε_{Nd} values and relatively high initial $^{87}Sr/^{86}Sr$ ratios. We suggest a subduction-modified refractory lithospheric mantle (phlogopite-bearing harzburgite or lherzolite) for these high-Mg potassic magmas. The Qianlishan diabases ($SiO_2 = 48.4$–48.7 wt %) are alkaline and have high TiO_2 and total Fe_2O_3 contents, together with the positive initial ε_{Nd} value, suggesting derivation from fertile asthenopheric mantle (phlogopite-bearing lherzolite). A back-arc extensional setting, related to subduction of the Palaeo-Pacific plate, is favoured to explain the petrogenesis of the Qianlishan granites and associated mafic dykes. Between 180 and 160 Ma, Southeast China was a continental arc, forming the 180–160 Ma plutons of the late Mesozoic volcanic-intrusive complex belt, and the lower-crust was granulitized. Since 160 Ma the northwestern belt has been in a back-arc extensional setting as a consequence of slab roll-back, resulting in the lithosphere thinning and an influx of asthenophere. The upwelling asthenosphere, on the one hand, induced the local lithospheric mantle to melt partially, forming high-Mg potassic magmas, and on the other hand it underwent decompression melting itself to form alkaline diabase magma. Pulsatory injection of such high-temperature magmas into the granulitized crustal source region induced them to partially melt and generate the A-type magmas of the Qianlishan granitic rocks.

Keywords: A-type granite, mafic dykes, back-arc extension setting, Qianlishan, SE China.

1. Introduction

During lateMesozoic times, extensive magmatism occurred in Southeast China, forming a belt of volcanic-intrusive complexes approximately 600 km wide, parallel to the present coastline (Fig. 1). Despite intensive scientific research, the geodynamic setting of these complexes remains controversial, and the focal question is whether the magmatism was associated with subduction of the Palaeo-Pacific plate (e.g. Zhou & Wu, 1994; Charvet, Lapierre & Yu, 1994; Martin, Bonin & Capdevila, 1994; Lapierre, Jahn & Charvet, 1997; Zhou & Li, 2000) or continental rifting and basin formation caused by collision between Indochina and South China during early Mesozoic times (e.g. Gilder *et al*. 1991; Li, 1999).

The Late Jurassic Qianlishan granites are distributed in the northwest of the volcanic-intrusive complex belt. They have attracted great interest due to their close relationship with the world-class Shizhuyuan W–Sn–Mo–Bi polymetallic deposit, but the petrogenesis of the granites remains controversial. Wang *et al*. (1987), Shen *et al*. (1995) and Mao *et al*. (1998) suggested that the Qianlishan granites are S-type rocks and may have been derived by partial melting of crustal rocks. However, Zhao *et al*. (2001) argued that the Qianlishan granites are not typical S-type, but are a sub-alkaline type, and that the significant mantle materials contributed to their genesis. Nevertheless, the detailed petrogenesis of the granites and their regional geodynamic implications are not well understood.

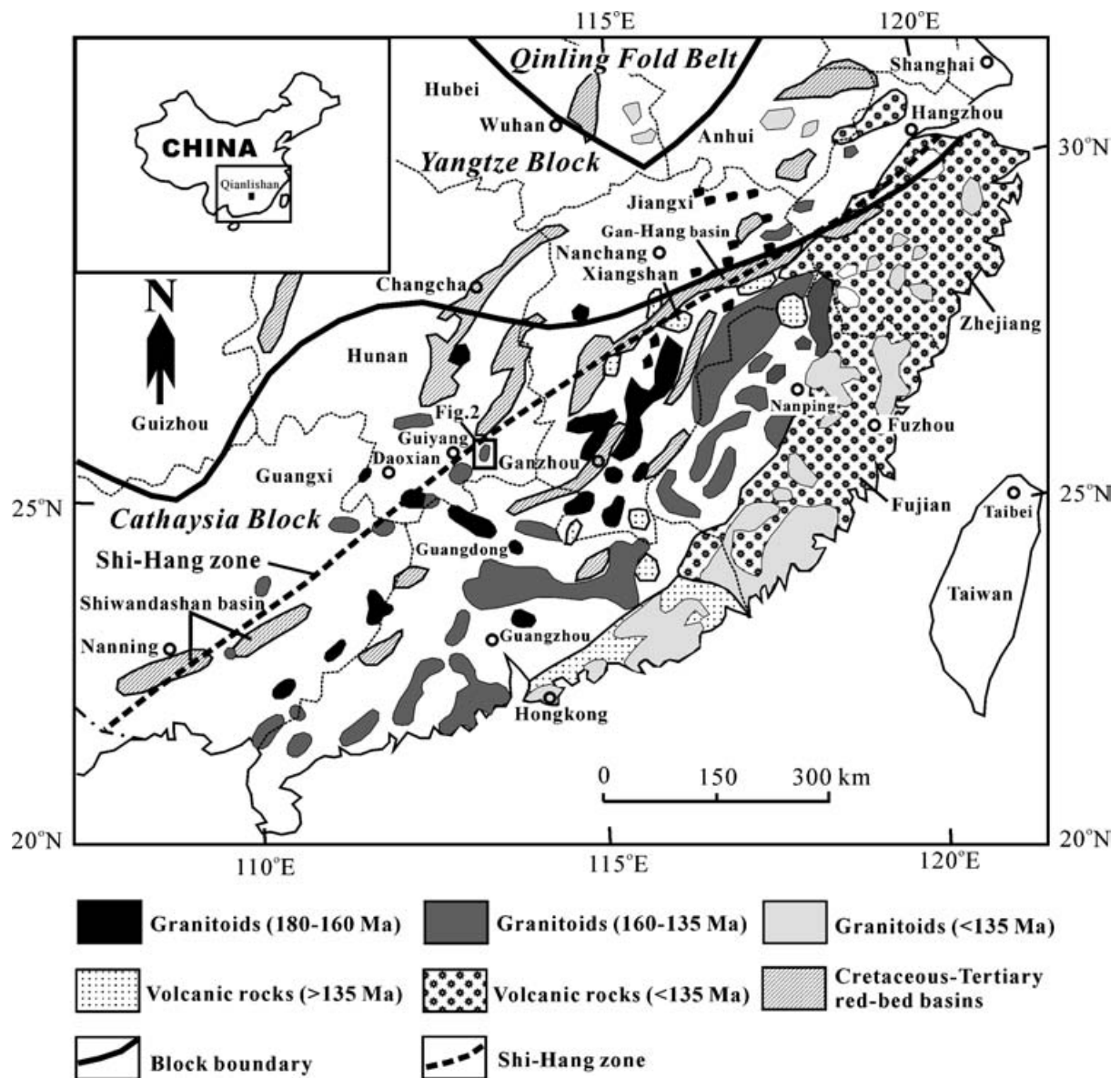* Author for correspondence: yhj186@hotmail.com

Figure 1. Sketch map showing the late Mesozoic belt of volcanic-intrusive complexes in SE China and geotectonic location of Qianlishan (modified after Gilder *et al.* 1996; Zhou & Li, 2000).

In this paper, we present new petrological and geochemical data for the Qianlishan granites and associated mafic dykes, in an attempt to constrain better both the petrogenetic processes and their significance in understanding the geodynamic setting of late Mesozoic tectonics and magmatism in Southeast China. These new data suggest that the Qianlishan granites belong to the A-type and that the mafic dykes are high-Mg potassic rocks, most probably generated in a back-arc extensional regime, related to subduction of the Palaeo-Pacific plate.

2. Geological setting

Qianlishan is located in Hunan Province, Southeast China (Fig. 1). A series of late Mesozoic volcanic-intrusive complexes were emplaced in Southeast China during three major stages from the early to late Yanshanian: 180–160 Ma; 160–135 Ma and 135–90 Ma (Zhou & Li, 2000). As indicated in Figure 1, the associated granitoids appear to young towards the coast.

A series of Cretaceous–Tertiary red-bed basins such as the Gan-Hang basin (the 'Gan-Hang Rift' of Gilder *et al.* 1996) and Shiwandashan basin formed concurrently with the latest phase of the regional magmatism (Fig. 1). These NE-trending basins are composed of red-coloured clastic rocks along with marl, gypsum and evaporites, locally interlayered with basalts. They are mainly located to the northwest of the volcanic-intrusive complex belt, and are thought to have been deposited in a back-arc extensional

environment (Zhou & Li, 2000). Bimodal mafic–felsic magmatism occurred in basins such as the Gan-Hang basin during Early Cretaceous times. A series of granite-porphyry dyke swarms intruded into the Early Cretaceous red beds. One of these granite-porphyries has a U–Pb zircon age of 105 ± 1 Ma (Yu, Ye & Wang, 2001). The mafic magmatism formed compact massive basalt lava flow sequences interbedded with Early Cretaceous red mudstone. Individual lava flows are around 10 m thick, with the thickest around 30 m. These basaltic rocks have K–Ar ages of 104–99 Ma (Yu, Ye & Wang, 2001) and are enriched in alkalis, light rare earth elements (LREE) and large ion lithophile elements (LILE); they belong to the shoshonitic series and were inferred by Liao *et al.* (1999) to be derived by partial melting of enriched lithospheric mantle. Gilder *et al.* (1996) proposed the name 'Shi-Hang zone' for this NE-trending zone of extensional basins, which are arguably parts of a single continental rift–shear-zone system.

The Qianlishan granitic pluton is located in the northwest of the volcanic-intrusive complex belt, and in the Shi-Hang zone (Fig. 1). It intruded into Devonian strata in the Late Jurassic (153–151 Ma) with an outcrop area of about 10 km^2. The intrusive body is composed of porphyritic biotite granite and equigranular biotite granite, and was intruded by granite-porphyry and mafic dykes (Fig. 2). Available geochronology for these rocks is summarized in Table 1.

Nearby coeval (152–146 Ma) mafic magmatism occurred in the Daoxian–Guiyang area near the Shi-Hang zone (Fig. 1). This includes the Daoxian basaltic lava and Guiyang (Zhicun) mafic dykes (Wang *et al.* 2003). These basaltic rocks (SiO$_2$ 45.0–52.7 wt%) have high MgO (6.8–17.9 wt%) and compatible element concentrations (e.g. Ni = 123–647 ppm), and high K$_2$O contents (most between 3.4 and 4.3 wt%), with K$_2$O/ Na$_2$O ratios of 1.7–4.2. The rocks have initial ε_{Nd} values of -0.7 to -3.8 and initial ^{87}Sr/^{86}Sr ratios of 0.7053–0.7070 (Wang *et al.* 2003). Wang *et al.* (2003) have suggested that these high-Mg potassic rocks (referred to below as the 'Guiyang mafic dykes') originated from an enriched mantle source, and did not experience significant crustal contamination during magma ascent.
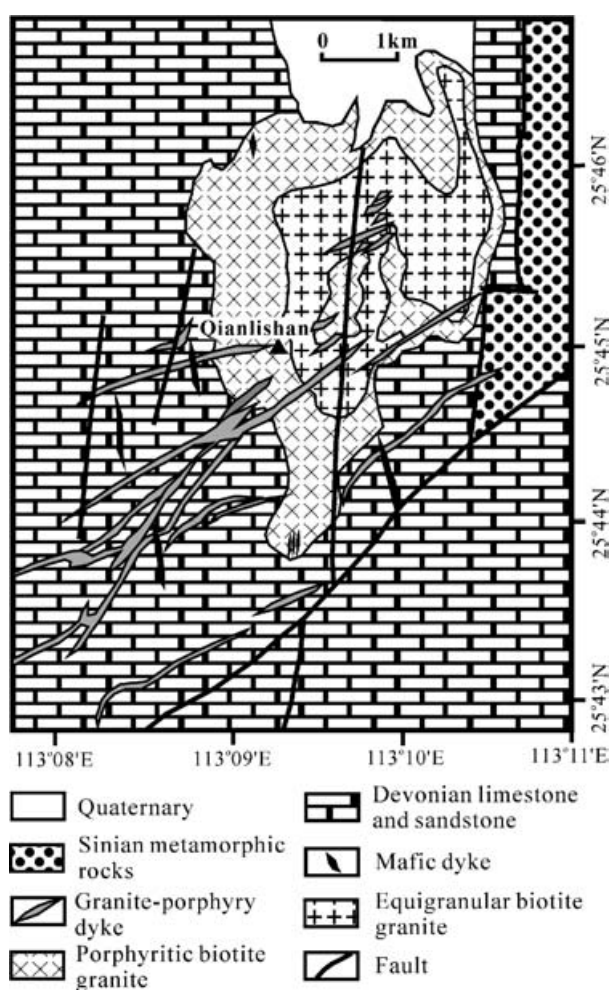

Figure 2. Simplified geological map of the Qianlishan granitic pluton.

3. Petrography

The porphyritic biotite granite (syenogranite, Fig. 3) is a light grey rock with a porphyritic texture (Fig. 4a). Phenocrysts (mostly 2–5 mm, $\sim 40\%$) include quartz ($\sim 20\%$), alkali feldspar ($\sim 10\%$) and plagioclase ($\sim 7\%$). The groundmass consists of alkali feldspar ($\sim 30\%$), quartz ($\sim 20\%$), plagioclase ($\sim 8\%$) and biotite ($\sim 5\%$) with a fine-grained (0.1–1.0 mm) granitic texture. Plagioclase is albite and usually

Table 1. A compilation of available isotope ages for the Qianlishan granitic rocks and mafic dykes in the area

| Lithology	Method/Mineral	Age (Ma)	References
Porphyritic biotite granite	SHRIMP U–Pb, zircon	153 ± 3	Li *et al.* 2004
Equigranular biotite granite	SHRIMP U–Pb, zircon	151 ± 3	Li *et al.* 2004
Granite-porphyry dyke	^{40}Ar–^{39}Ar, K-feldspar	144 ± 3	Liu *et al.* 1997
Mafic dyke in Qianlishan	^{40}Ar–^{39}Ar, whole rock	142 ± 3	Liu *et al.* 1997
Mafic dyke in Guiyang	K–Ar, whole rock	146 ± 2	Wang *et al.* 2003
Basic lava in Daoxian	^{40}Ar–^{39}Ar, whole rock	152 ± 1	Wang *et al.* 2003
Basic lava in Daoxian	^{40}Ar–^{39}Ar, whole rock	147 ± 0.3	Wang *et al.* 2003
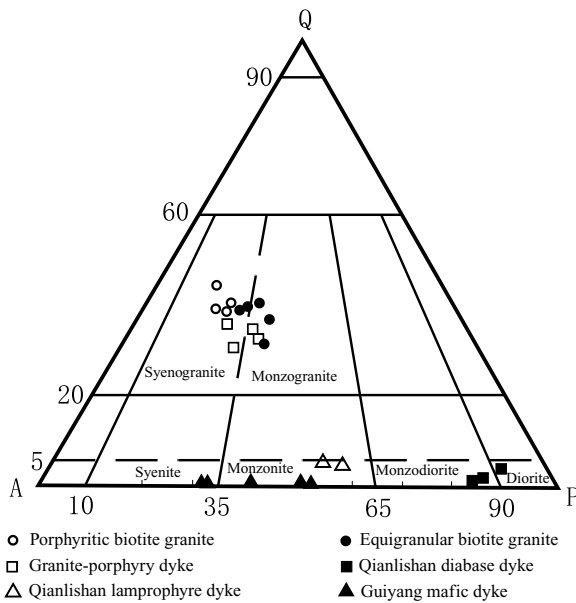
Figure 3. QAP Classification diagram for the Qianlishan granitic rocks and mafic dykes (Streckeisen, 1976). Q, A and P denote quartz, alkaline feldspar and plagioclase, respectively. Original data for the Guiyang mafic dykes are from Wang *et al*. (2003).

sericitized. Alkali feldspar is also locally sericitized. Biotite is locally altered to chlorite. Accessory minerals include zircon, monazite, xenotime, thorite and apatite.

The equigranular biotite granite (monzogranite-syenogranite, Fig. 3) is a light grey rock with a medium-grained (mostly 2–5 mm) granitic texture (Fig. 4b), consisting of alkali feldspar ($\sim 40\%$), quartz ($\sim 38\%$), plagioclase ($\sim 19\%$), biotite ($\sim 3\%$) and minor accessory minerals such as zircon, thorite, monazite, yttrofluorite and ilmenite. Plagioclase (albite) and alkali feldspar are locally sericitized. Biotite is usually altered to chlorite.

The rocks of granite-porphyry dykes are light purplish-red in colour, and have mineral components of monzogranite and syenogranite (Fig. 3). They show a typical porphyritic texture (Fig. 4c) with phenocrysts (mostly 5–20 mm, $\sim 30\%$) of alkali feldspar, plagioclase and quartz. The quartz phenocrysts show resorption textures (Fig. 4c). The groundmass has a microcrystalline texture and consists of alkali feldspar, quartz, plagioclase and biotite. Plagioclase is oligoclase and is generally sericitized. Alkali feldspar is also sericitized. Biotite is locally altered to chlorite.
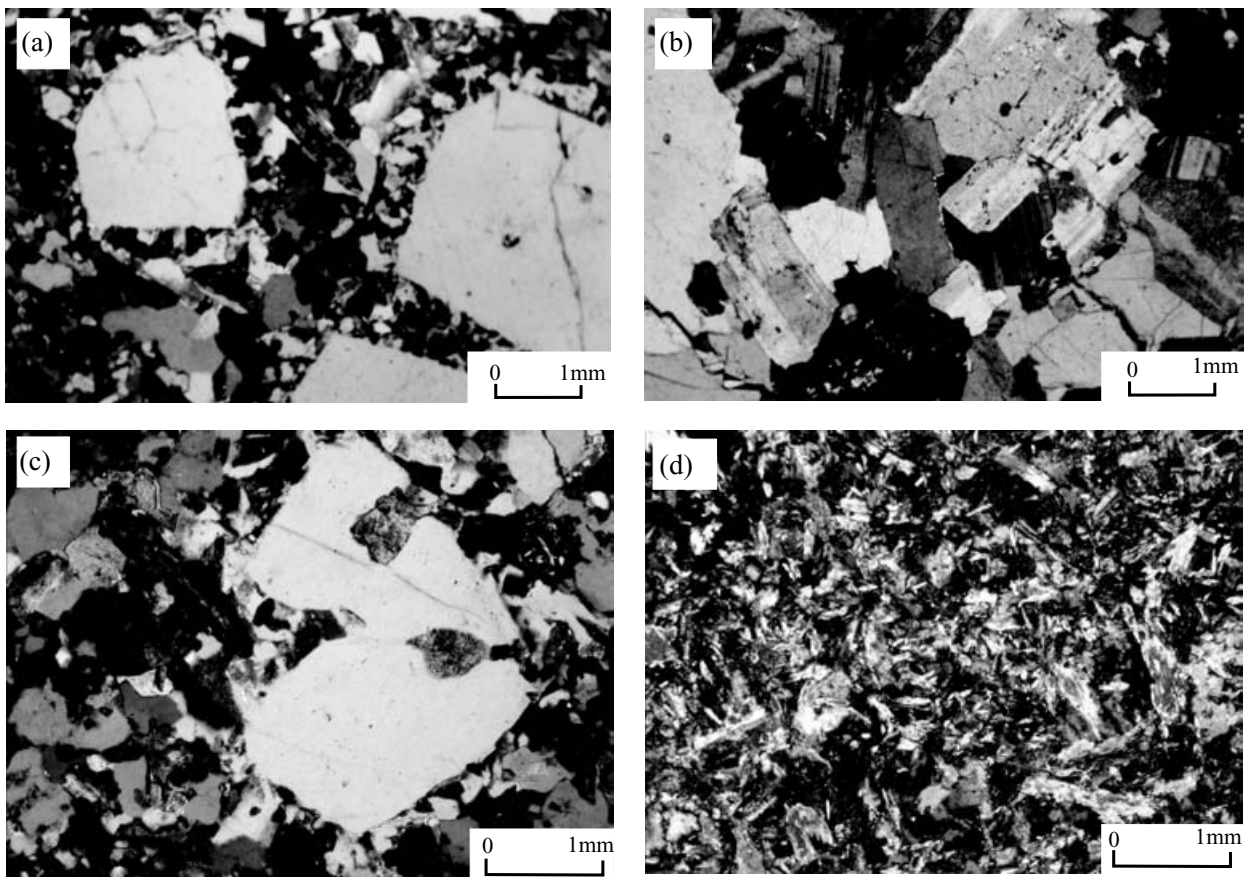

Figure 4. Petrographical photos showing a porphyritic texture for porphyritic biotite granite (a), a medium-grained granitic texture for equigranular biotite granite (b), a porphyritic texture for granite-porphyry dyke (c), and a microcrystalline texture for lamprophyre dyke (d).

Table 2. Representative microprobe analyses of biotite in the Qianlishan granitic rocks

Rock type	Porphyritic biotite granite			Equigranular biotite granite				Granite-porphyry dyke			
Sample	164[*]	166[*]	167[*]	SZY-9	SZY-9	SZY-9	SZY-9	SZY-21	SZY-21	SZY-21	SZY-21
SiO_2	36.97	36.98	37.20	40.18	40.50	42.14	41.81	39.15	40.43	40.82	37.70
TiO_2	2.19	2.10	1.93	0.60	0.50	0.01	0.35	2.14	1.99	2.12	2.30
Al_2O_3	20.12	19.85	19.99	25.03	23.76	24.06	24.69	15.71	16.89	16.54	17.29
FeO	21.60	22.16	22.84	20.03	20.02	17.67	16.65	17.47	17.63	16.95	18.94
MnO	1.05	0.96	0.95	1.55	1.62	1.40	1.48	0.62	0.37	0.58	0.45
MgO	3.44	3.76	3.42	0.09	0.09	0.06	0.10	10.25	10.41	10.96	9.65
CaO	–	0.03	0.02	0.04	0.03	0.04	0.03	0.04	0.03	0.04	–
Na_2O	0.20	0.22	0.14	0.08	0.06	0.07	0.06	0.13	0.07	0.13	0.07
K_2O	9.74	9.82	9.78	10.00	9.85	9.88	9.78	9.87	9.92	9.80	9.30
Sum	95.31	95.88	96.27	97.59	96.42	95.33	94.96	95.38	97.74	97.93	95.70
Cations per 23 oxygens											
Si	5.934	5.920	5.940	6.152	6.278	6.492	6.434	6.106	6.147	6.178	5.955
Ti	0.264	0.253	0.232	0.069	0.059	0.001	0.041	0.251	0.227	0.241	0.232
Al^{IV}	2.066	2.080	2.060	1.848	1.722	1.508	1.566	1.894	1.853	1.822	2.045
Al^{VI}	1.737	1.662	1.699	2.666	2.615	2.857	2.907	0.992	1.171	1.126	1.056
Fe^{3+}[**]	0	0	0	0	0	0	0	0.396	0.168	0.140	0.374
Fe^{2+}	2.899	2.967	3.050	2.565	2.596	2.277	2.142	1.882	2.073	2.006	2.127
Mn	0.143	0.130	0.128	0.200	0.213	0.182	0.193	0.082	0.048	0.074	0.060
Mg	0.823	0.897	0.814	0.020	0.020	0.014	0.024	2.383	2.359	2.474	2.272
Ca	–	0.005	0.003	0.007	0.004	0.006	0.005	0.006	0.006	0.007	–
Na	0.062	0.068	0.043	0.024	0.018	0.022	0.019	0.038	0.021	0.037	0.022
K	1.994	2.005	1.992	1.953	1.947	1.941	1.921	1.964	1.924	1.893	1.874
Sum	15.922	15.987	15.961	15.504	15.472	15.300	15.252	15.994	15.997	15.998	16.017
Mg no.	0.22	0.23	0.21	0.01	0.01	0.01	0.01	0.51	0.51	0.54	0.48

[*] Original data from Mao *et al.* (1998); [**]using surplus oxygen method to allocate the iron following the method of Zheng (1983); – = below limit of detection; Mg no. = $Mg/(Mg + Fe_T)$.

Accessory minerals include allanite, apatite, rutile, zircon, monazite, ilmenite and fluorite.

The mafic dykes in the studied area include diabase and lamprophyre. They are greyish-black rocks and have mineral components of diorite, monzodiorite and monzonite (Fig. 3). The diabase shows a typical porphyritic texture with phenocrysts of plagioclase (mostly 1–5 mm, ~ 25 %) and quartz (~ 1 mm, ~ 3 %). The groundmass consists of plagioclase, pyroxene and glass with an interstitial texture. Plagioclase is labradorite (phenocryst) and oligoclase (matrix) and has been variably sericitized. The lamprophyre is composed of amphibole (~ 55 %), plagioclase (~ 25 %), alkali feldspar (~ 15 %) and quartz (~ 5 %) with a micro-crystalline texture (Fig. 4d). Plagioclase is andesine and locally sericitized.

4. Mineral chemistry

Electron microprobe analysis has been carried out on biotite, plagioclase and K-feldspar from the Qianlishan granitic rocks and mafic dykes, using a JEOL JXA-8800 Superprobe at the State Key Laboratory for Mineral Deposits Research in Nanjing University. Operating conditions were 15 kV at 10 nA beam current. For biotite, the standards used were hornblende (for Si, Ti, Al, Fe, Ca, Mg, Na and K) and fayalite (for Mn). For feldspar, the standards used were hornblende (for Si, Ti, Al, Fe, Ca and Mg), albite (for Na), orthoclase (for K) and fayalite (for Mn). The results are presented in Tables 2 and 3, and illustrated in Figure 5.

Biotite in the porphyritic granite is Fe-rich ferri-biotite and annite (siderophyllite) (Fig. 5a). Biotite in the equigranular granite has a higher Al_2O_3 content than the biotite in the porphyritic granite and plots in the alumino-mica field (Fig. 5a). The granite-porphyry dyke contains the magnesio-biotite (Fig. 5a), which has higher Mg no. (0.48–0.54) than biotites in the porphyritic and equigranular granites (0.01–0.23) (Table 2).

Plagioclases in the porphyritic and equigranular granite are albite, and plagioclase in the granite-porphyry dyke is oligoclase (Fig. 5b). The mafic dykes contain more calcic plagioclase with andesine in the lamprophyre and labradorite (phenocryst) and oligoclase (matrix) in the diabase (Table 3, Fig. 5b). All the alkali feldspars have high contents of Or (82–98 %) with minor amounts of Ab (2–18 %) and negligible amounts of An (0.2–1.2 %) (Table 3, Fig. 5b).

5. Whole-rock geochemistry

Twenty samples of the Qianlishan granitic rocks and mafic dykes have been collected. After petrographic examination, the freshest 14 samples were selected for whole-rock geochemical analysis. Geochemical data were determined at the Centre of Modern Analysis, Nanjing University, by X-ray fluorescence analysis for major elements and at the State Key Laboratory for Mineral Deposits Research, Nanjing University, by inductively coupled plasma mass spectrometry (ICP-MS)

Table 3. Representative microprobe analyses of feldspar in the Qianlishan granitic rocks and mafic dykes

Rock type	Porphyritic biotite granite				Equigranular biotite granite			Granite-porphyry dyke				Diabase dyke		Lamprophyre dyke	
Sample	JCT-29	JCT-29	JCT-29	JCT-29	SZY-9	SZY-9	SZY-9	SZY-21	SZY-21	SZY-21	SZY-21	JCT-28	JCT-28	SZY-11	SZY-11
Mineral	Pl (P)	Pl (M)	Kfs (P)	Kfs (M)	Pl	Pl	Kfs	Pl (P)	Pl (M)	Kfs (P)	Kfs (M)	Pl (P)	Pl (M)	Pl	Kfs
SiO_2	68.74	68.23	63.87	63.92	67.92	68.51	64.25	62.93	63.90	64.44	64.55	53.95	62.47	56.43	63.12
TiO_2	–	–	–	0.01	–	–	–	–	–	–	–	0.03	0.88	–	0.02
Al_2O_3	20.54	20.67	18.98	19.53	20.21	19.51	17.74	24.25	24.08	18.71	18.36	28.76	22.49	27.64	18.16
FeO	–	0.02	–	–	–	0.07	0.02	0.12	0.07	0.02	0.05	0.41	0.54	0.74	0.39
MnO	0.03	0.02	0.01	–	0.01	0.01	–	0.03	0.02	0.02	0.04	0.04	0.02	0.04	0.04
MgO	–	–	–	–	0.01	0.01	–	0.02	–	–	–	0.12	0.14	0.16	–
CaO	0.19	0.10	0.03	0.03	0.93	0.16	–	5.27	3.35	0.02	–	11.88	3.45	6.94	0.25
Na_2O	11.12	11.70	0.18	1.94	10.76	10.94	0.31	8.40	8.05	0.44	0.27	4.34	8.37	5.30	0.56
K_2O	0.06	0.08	16.43	13.85	0.28	0.11	16.42	0.43	0.45	15.87	16.47	0.23	0.36	2.49	16.16
Total	100.68	100.81	99.51	99.28	100.13	99.31	98.74	101.45	99.92	99.51	99.75	99.77	98.72	99.73	98.7
Cations per 32 oxygens															
Si	11.900	11.831	11.883	11.814	11.864	12.016	12.047	11.006	11.227	11.950	11.980	9.784	11.183	10.214	11.890
Ti	–	–	–	0.001	–	–	–	–	–	–	–	0.004	0.118	–	0.003
Al	4.188	4.221	4.158	4.252	4.156	4.030	3.917	4.995	4.983	4.085	4.013	6.142	4.742	5.892	4.029
Fe^{2+}	–	0.002	–	–	–	0.010	0.003	0.018	0.011	0.003	0.007	0.063	0.081	0.112	0.061
Mn	0.004	0.002	0.002	–	0.001	0.001	–	0.005	0.002	0.003	0.006	0.006	0.002	0.006	0.006
Mg	–	–	–	–	0.002	0.002	–	0.004	–	–	–	0.034	0.038	0.043	–
Ca	0.036	0.019	0.006	0.006	0.174	0.031	–	0.987	0.630	0.003	0	2.309	0.662	1.346	0.051
Na	3.734	3.935	0.066	0.696	3.645	3.722	0.112	2.850	2.742	0.157	0.098	1.527	2.906	1.859	0.206
K	0.012	0.017	3.900	3.266	0.063	0.024	3.927	0.096	0.101	3.755	3.900	0.053	0.083	0.575	3.885
Total	19.874	20.027	20.015	20.035	19.905	19.836	20.006	19.961	19.696	19.956	20.004	19.922	19.815	20.047	20.131
An	1.0	0.5	0.2	0.2	4.5	0.8	0	25.1	18.1	0.1	0	59.4	18.1	35.6	1.2
Ab	98.7	99.1	1.7	17.5	93.9	98.5	2.8	72.5	79.0	4.0	2.5	39.3	79.6	49.2	5.0
Or	0.3	0.4	98.2	82.3	1.6	0.6	97.2	2.4	2.9	95.9	97.5	1.4	2.3	15.2	93.8

Pl = plagioclase; Kfs = K-feldspar; P = phenocryst; M = matrix; – = below limit of detection.
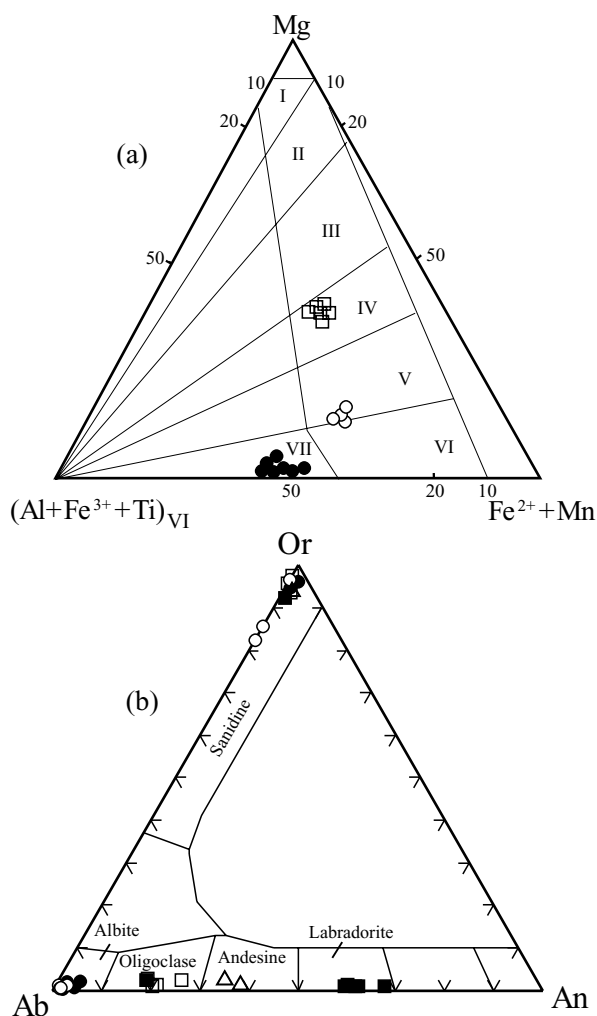
Figure 5. (a) Classification diagram for biotite (Foster, 1960). I – phlogopite; II – iron-phlogopite; III – eastonite; IV – magnesio-biotite; V – ferri-biotite; VI – annite (siderophyllite); VII – alumino-mica. (b) Ternary classification diagram for feldspar (Deer, Howie & Zussman, 1992). Ab – albite, An – anorthite, Or – orthoclase. Symbols as in Figure 3.

Figure 6. (a) Alkalinity ratio (AR) v. SiO_2 (Wright, 1969), where $AR = (Al_2O_3 + CaO + (Na_2O + K_2O))/(Al_2O_3 + CaO - (Na_2O + K_2O))$ (wt %); (b) K_2O v. SiO_2. Symbols as in Figure 3. Original data for the Guiyang mafic dykes are from Wang *et al.* (2003).

using a Finnigan Element II system for trace elements and by the conventional BrF_5 extraction method for oxygen isotopic compositions. Sr and Nd isotopic compositions were measured in the Open Laboratory for Isotope Geology of the Chinese Academy of Geological Sciences (Beijing), following the methods of Zhang, Liu & Fu (1994). $^{143}Nd/^{144}Nd$ ratios were normalized to $^{146}Nd/^{144}Nd = 0.7219$ and $^{87}Sr/^{86}Sr$ ratios to $^{86}Sr/^{88}Sr = 0.1194$. During the period of analysis, measurements for the laboratory J.M. Nd_2O_3 and NBS-987 Sr standards yielded results of $^{143}Nd/^{144}Nd$ ratio of 0.511126 ± 9 (2σ, n = 27) and $^{87}Sr/^{86}Sr$ ratio of 0.710228 ± 14 (2σ, n = 30), respectively. Total analytical blanks were 5×10^{-11} g for Sm and Nd and $(2–5) \times 10^{-10}$ g for Rb and Sr. The results are listed in Table 4.
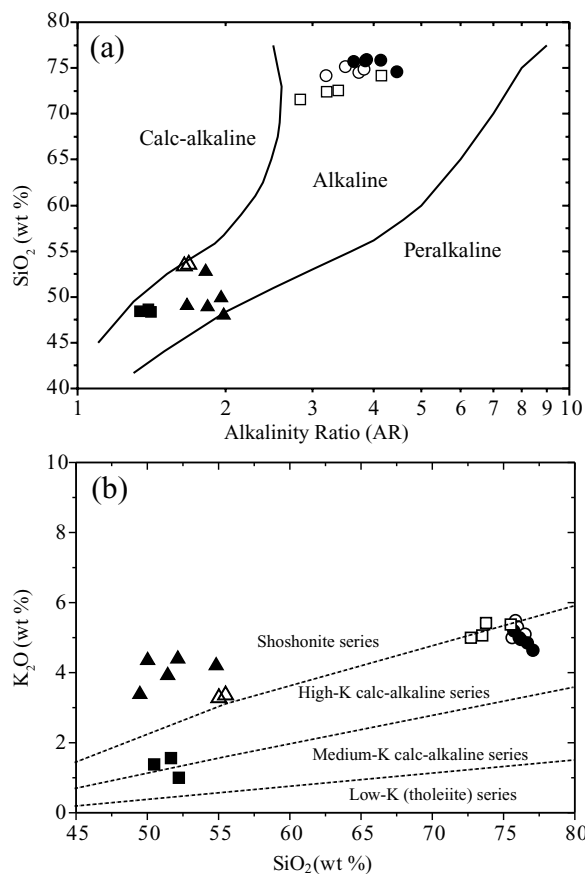
5.a. Granitic rocks

The porphyritic and equigranular biotite granites have high SiO_2 contents in the range of 74.5 to 75.9 wt %. The granite-porphyry dykes show slightly lower SiO_2 contents (71.6–74.2 wt %) than the granites (Table 4). The granites are slightly peraluminous with alumina saturation index ASI (= molar $Al_2O_3/(CaO + Na_2O + K_2O)$) from 1.00 to 1.05, whereas the granite-porphyry dykes are metaluminous with ASI < 1.00 (Table 4). These granitic rocks are all alkali-rich, with all data plotting in the alkaline field (Fig. 6a). They also have high K_2O contents with most data plotting in the high-K calc-alkaline field in terms of K_2O v. SiO_2 (Fig. 6b).

The granitic rocks have high REE contents (339–670 ppm, Table 4), but are depleted in Eu, showing notable negative Eu anomalies (Fig. 7a, b). These granitic rocks also have high Ga (16–29 ppm) and high field strength elements (HFSE) (e.g. Nb, 23–82 ppm; Y, 37–250 ppm) contents. The granitic rocks are depleted in Ba and Sr, showing notable negative Ba and Sr anomalies (Fig. 8a).

Table 4. Representative chemical and isotopic compositions of the Qianlishan granitic rocks and mafic dykes

Rock type	Porphyritic biotite granite		Equigranular biotite granite			Granite-porphyry dyke				Diabase	Lamprophyre		Guiyang mafic dyke[*]	
Sample	JCT-29	SZY-19	SZY-1	SZY-20	SZY-9	JCT-15	JCT-27	SZY-18	SZY-21	JCT-28	SZY-11a	SZY-11b	ZHC-4	ZHC-13
SiO_2	74.49	74.87	75.86	75.92	74.62	72.57	74.17	72.42	71.56	48.66	53.75	53.54	52.73	47.92
TiO_2	0.12	0.11	0.05	0.05	0.01	0.25	0.12	0.31	0.27	2.13	0.95	0.93	0.64	0.56
Al_2O_3	12.81	12.60	12.67	12.41	13.55	13.47	12.73	13.29	13.84	15.36	12.48	13.14	12.71	9.08
Fe_2O_3	0.45	0.50	0.52	0.84	0.09	0.33	0.17	0.87	0.83	3.68	3.13	2.93	3.00	5.60
FeO	1.02	1.03	0.50	0.44	0.15	0.94	1.31	1.39	1.03	6.52	4.87	4.87	3.67	4.90
MnO	0.04	0.04	0.03	0.03	0.01	0.04	0.04	0.04	0.04	0.15	0.30	0.29	0.18	0.15
MgO	0.14	0.17	0.12	0.15	0.09	0.37	0.15	0.40	0.44	4.60	8.35	8.14	6.64	15.24
CaO	1.11	1.16	0.90	0.85	0.88	1.95	1.09	1.80	2.51	7.94	7.45	7.05	9.58	6.65
Na_2O	2.65	2.82	3.49	3.24	4.02	3.06	3.17	2.94	2.91	2.90	1.76	1.75	2.43	1.00
K_2O	5.39	5.23	4.80	4.57	5.12	5.33	5.28	4.99	4.92	0.93	3.29	3.21	4.04	4.17
P_2O_5	0.03	0.03	0.01	0.01	0.01	0.07	0.03	0.08	0.07	0.31	0.49	0.53	0.55	0.53
LOI	1.14	1.18	0.50	1.08	0.96	0.98	0.99	1.06	1.34	6.19	3.03	3.03	3.30	3.75
Total	99.37	99.73	99.45	99.60	99.51	99.36	99.23	99.59	99.76	99.38	99.85	99.42	99.47	99.55
ASI	1.05	1.02	1.01	1.05	1.00	0.94	0.99	0.98	0.94	0.76	0.62	0.68	0.49	0.50
Sc	2.3	2.5	3.9	4.2	2.8	6.2	2.4	4.5	4.7	23	21	14	19	22
V	3.4	3.5	2.1	2.7	1.9	19	5.4	27	21	245	180	178	151	137
Ga	21	23	25	26	29	19	23	16	16	20	18	16		
Rb	458	687	695	697	962	743	735	335	509	88	3806	2756	205	151
Sr	25	25	10	14	11	101	31	73	102	318	335	241	578	567
Y	56	74	122	95	250	58	69	48	37	21	34	29	21	18
Zr	134	153	77	72	121	158	194	418	141	148	191	188	159	114
Nb	23	41	36	43	82	53	49	56	41	16	18	18	34	13
Cs	19	16	31	18	14	42	33	15	30	7.1	15	8.8		
Ba	54	53	14	19	7.7	253	98	190	169	310	405	360	1759	1359
La	74	122	29	70	38	108	135	148	76	37	35	37	41	24
Ce	138	261	62	131	108	233	293	289	168	86	82	87	76	48
Pr	12.4	23.5	9.3	18.5	12.1	22.4	26.3	25.5	15.1	8.7	10.2	10.2	8.6	5.7
Nd	51.5	74.8	33.4	68.3	49.0	73.5	85.1	79.2	48.8	33.4	43	43	33.9	23.4
Sm	10.3	11.4	11.7	15.7	15.4	10.5	12.6	10.2	7.0	5.5	9.2	8.5	6.8	4.6
Eu	0.31	0.27	0.11	0.12	0.01	0.89	0.41	0.95	0.75	1.91	2.4	2.1	1.57	1.13
Gd	9.3	8.0	14.7	10.6	11.2	7.6	8.8	7.8	4.4	4.2	8.6	8.1	5.6	4.0
Tb	1.29	2.66	3.07	4.28	5.54	2.36	2.90	2.01	1.33	1.18	1.25	1.19	0.74	0.58
Dy	9.9	13.5	20.9	23.5	29.3	11.8	14.4	8.8	6.6	5.6	6.9	6.1	4.2	3.3
Ho	2.10	2.76	4.34	4.73	5.99	2.46	3.01	1.63	1.41	1.15	1.16	1.07	0.76	0.65
Er	6.05	9.00	12.69	14.4	19.9	8.25	9.30	5.06	4.57	3.46	3.4	2.9	2.07	1.79
Tm	0.87	1.17	2.01	1.85	3.03	1.13	1.25	0.67	0.61	0.40	0.45	0.40	0.32	0.27
Yb	6.22	6.43	12.2	10.0	18.3	6.9	6.8	4.2	3.47	2.12	2.7	2.4	2.03	1.65
Lu	0.92	1.34	1.68	1.91	3.81	1.40	1.39	0.85	0.73	0.43	0.44	0.37	0.32	0.24
Hf	4.8	6.7	4.7	4.7	11.7	6.3	8.2	15.5	4.4	4.2	5.1	4.8	4.4	3.2
Ta	3.9	4.7	8.9	7.9	9.2	7.5	4.0	6.4	3.5	0.73	1.84	1.76	1.7	0.73
Pb	43	55	34	72	35	31	53	67	26	24	7.6	5.5	23	12
Th	64	80	38	39	50	60	71	190	50	2.1	14	13	12	4.3
U	19	25	27	28	48	34	20	50	20	0.64	5.7	5.2	4.0	0.87
Total REE	378	612	339	471	569	548	670	631	376	212	240	238	206	138
Rb/Sr	18.31	27.61	68.98	48.72	88.05	7.34	23.80	4.60	5.01	0.28	1.14	1.14	0.35	0.27
Ba/Rb	0.12	0.08	0.02	0.03	0.01	0.34	0.13	0.57	0.33	3.53	1.06	1.31	8.58	8.99
Sm/Nd	0.20	0.15	0.35	0.23	0.31	0.14	0.15	0.13	0.14	0.17	0.21	0.20	0.20	0.20
Nb/U	1.24	1.63	1.35	1.52	1.73	1.56	2.50	1.10	2.07	24.53	3.22	3.44	8.57	15.10
Ce/Pb	3.17	4.76	1.84	1.81	3.10	7.46	5.52	4.29	6.44	3.51	10.79	15.61	3.37	3.99
$\delta^{18}O$ (‰)	7.0		7.2	8.7		7.3	9.3	7.0						
$^{87}Sr/^{86}Sr_{(T)}$	0.7072–0.7097		0.7122–0.7182			0.7129–0.7147				0.708610	0.707720		0.7053–0.7070	
ε_{Nd} (T)	− 6.4∼ − 7.6		− 7.4∼ − 11.5			− 5.0∼ − 8.5				+0.5	− 1.1		− 0.7∼ − 3.8	
T_{DM}, Ma	1949–2632		Minus values			1284–1578								

[*] Data from Wang *et al*. (2003); original data for Sr–Nd isotopic compositions of the Qianlishan granitic rocks from Mao *et al*. (1998).
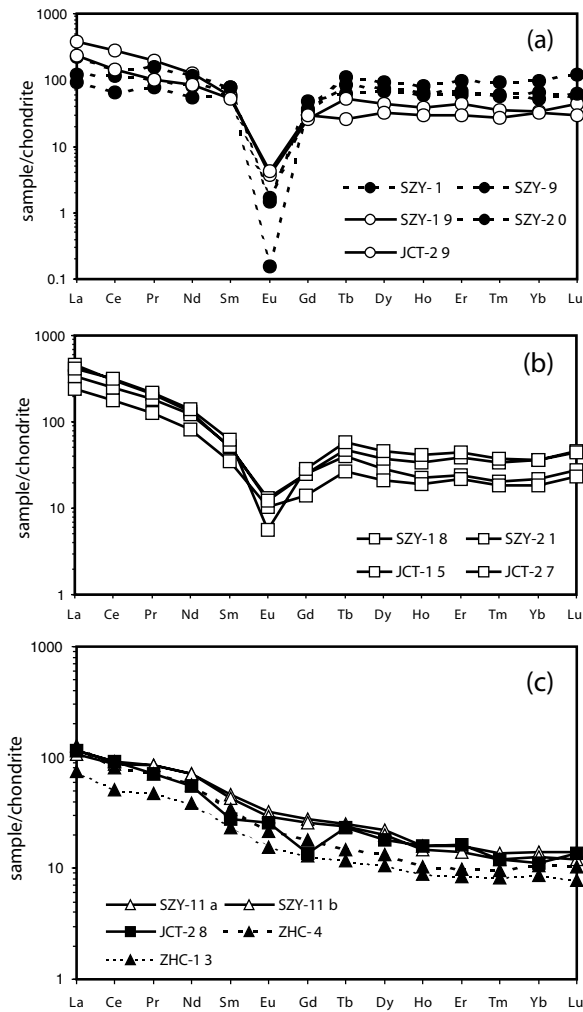
Figure 7. Chondrite-normalized REE patterns of the Qianlishan biotite granites (a), granite-porphyry dykes (b) and mafic dykes (c). Symbols as in Figure 3. Original data for the Guiyang mafic dykes are from Wang *et al.* (2003).

The granitic rocks have ε_{Nd} (T) values of −5.0 to −11.5, initial [87]Sr/[86]Sr ratios of 0.7072–0.7182 and $\delta^{18}O$ values of 7.0–9.3 ‰ (Table 4). Their Nd and Sr isotopic compositions are between those of Palaeo- to Mesoproterozoic orthometamorphic and parametamorphic rocks occurring in the Cathaysia Block (Fig. 9a).

5.b. Mafic dykes

The Qianlishan and neighbouring Guiyang mafic dykes are all enriched in alkalis (Fig. 6a), and have high K_2O contents with the data plotting in the field of the shoshonite series except for the Qianlishan diabases that have relatively low K_2O contents (Fig. 6b). They are enriched in LREE (Fig. 7c), LILE and depleted in HFSE (Fig. 8b). These mafic rocks have high MgO and compatible element contents (e.g. Sc = 19–27 ppm, V = 137–255 ppm, Table 4), suggesting equilibration of the primitive magma with mantle peridotite (Hickey & Frey, 1982; Bloomer & Hawkins, 1987). This also
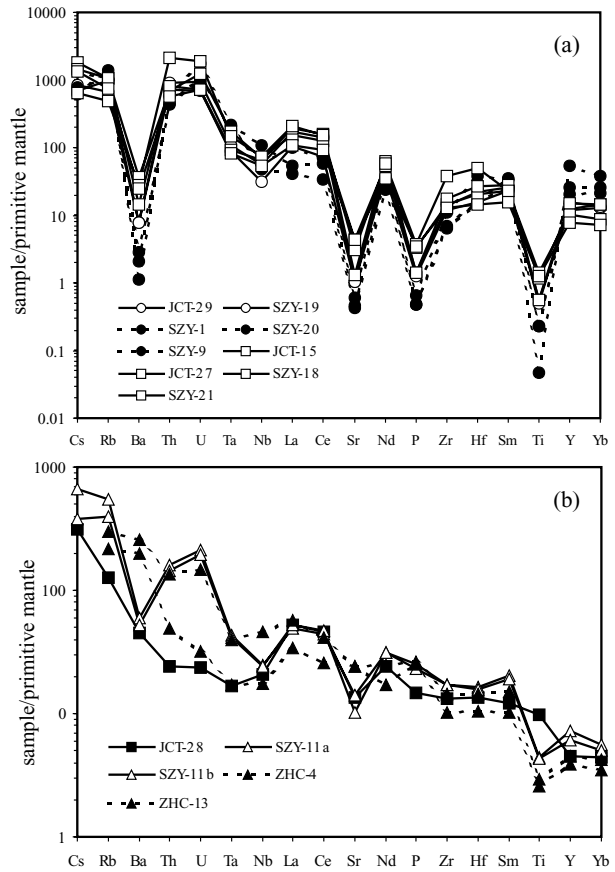
Figure 8. Primitive mantle-normalized trace element patterns of the Qianlishan granitic rocks (a) and mafic dykes (b). Symbols as in Figure 3. Original data for the Guiyang mafic dykes are from Wang *et al.* (2003).

implies that these mafic rocks do not experience significant fractionation or crustal assimilation in their petrogenesis and thus most probably represent the mantle-derived primitive magmas. The Qianlishan lamprophyre dyke has a relatively low ε_{Nd} (T) value of −1.1 and high initial [87]Sr/[86]Sr ratio of 0.7077, consistent with the Guiyang mafic dykes that show ε_{Nd} (T) values of −0.7 to −3.8 and initial [87]Sr/[86]Sr ratios of 0.7053–0.7070 (Table 4), suggesting an enriched mantle source for the origin of these magmas (Fig. 9b). However, the Qianlishan diabase has a relatively high ε_{Nd} (T) value of +0.5 and initial [87]Sr/[86]Sr ratio of 0.7086, suggesting a distinct origin. See below for more discussion.

6. Discussion

6.a. Origin of granitic rocks

6.a.1. S-type v. A-type

In traditional classification schemes, the granitic rocks may be divided into the I-, S-, M- and A-types (Chappell & White, 1974; Collins, Beams & White, 1982; Pitcher, 1983). Later, Eby (1992) proposed that
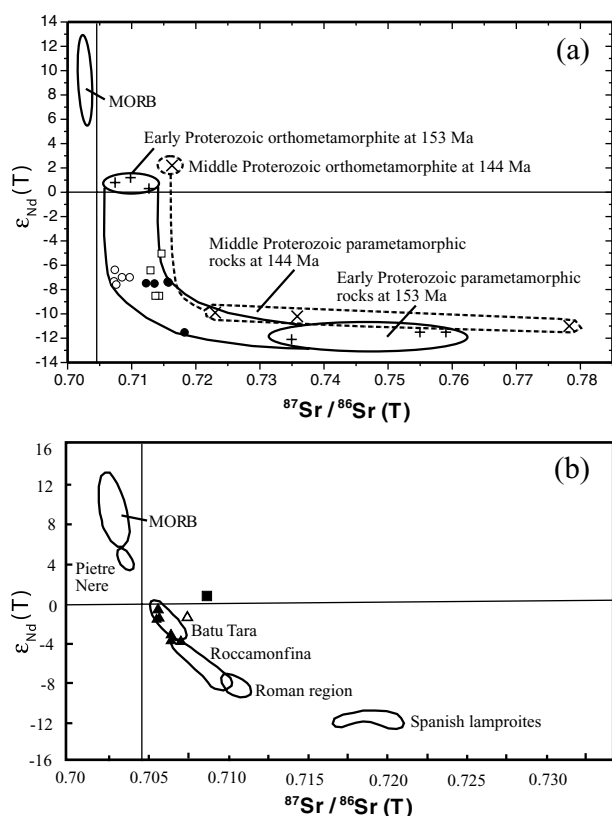
Figure 9. Initial Nd–Sr isotopic diagram for the Qianlishan granitic rocks (a) and mafic dykes (b). Pietre Nere, Batu Tara, Roccamonfina, Roman region and Spanish lamproites represent orogenic potassic rocks, which plot along a mixing line between an upper mantle end-member having Sr and Nd isotopic compositions similar to mid-ocean ridge basalts (MORB), and an enriched mantle end-member having Sr and Nd isotopic compositions similar to those of oceanic sediments (Nelson, 1992). The original Nd–Sr isotopic compositions of Qianlishan granitic rocks from Mao *et al.* (1998), Guiyang mafic dykes from Wang *et al.* (2003), Early Proterozoic metamorphic rocks from Yuan *et al.* (1991) and Middle Proterozoic metamorphic rocks from G. R. Hu (unpub. Ph.D. thesis, Nanjing Univ. 1998). Symbols as in Figure 3.

the A-type could be further divided into A_1 and A_2 subtypes.

In terms of the rock series, the S-type granites are calc-alkaline with ASI > 1.1, whereas the A-type granites belong to alkaline and peralkaline series with ASI no more than 1.05. Petrographically, the notable characteristics of S-type granites are the abundance of Al-rich minerals such as muscovite, garnet and cordierite, whereas the mafic minerals in A-type granites generally include Fe-rich biotite and calcic amphibole for the A_2 subtype or sodic amphibole and pyroxene for the A_1 subtype (Jiang *et al.* 2002). In terms of composition, the A-type granites have higher alkalis, REE and HFSE concentrations and higher Ga/Al ratios, and lower Al_2O_3, CaO and MgO concentrations than the S-type granites (Whalen, Currie & Chappell, 1987).

Obviously, the characteristics of the Qianlishan granitic rocks, with Fe-rich biotite (Fig. 5a), enrichment in alkalis (Fig. 6a), REE (except for Eu, Fig. 7a, b) and HFSE, with high Ga/Al ratios (Fig. 10a, b, c), strongly suggest an A-type affinity. High Rb/Nb and Y/Nb ratios of these rocks (Fig. 10d) further suggest that they belong to the A_2 group of Eby (1992).

6.a.2. Isotopic constraints

Petrogenetic models for A-type magmas have involved either partial melting of specific crustal protoliths (e.g. Collins, Beams & White, 1982; Whalen, Currie & Chappell, 1987; Creaser, Price & Wormald, 1991), or extensive fractional crystallization from mantle-derived basaltic magmas (e.g. Turner, Foden & Morrison, 1992). At Qianlishan, the Sr–Nd isotopic compositions of the granitic rocks are different from those of coeval mafic rocks (Fig. 9), which therefore rules out the extensive fractional crystallization from coeval mafic magmas for the origin of the Qianlishan A-type granites. Instead, these A-type granitic rocks show a close relationship to Palaeo- to Mesoproterozoic basement metamorphic rocks in terms of Sr–Nd isotopic compositions (Fig. 9a), suggesting that they were most probably derived from these crustal rocks.

There is no argument that the Cathaysia Block has a Palaeo- to Mesoproterozoic basement, which is exposed mainly in the eastern Jiangxi, northern Guangxi and northwestern Fujian Provinces (e.g. Yuan *et al.* 1991; Li *et al.* 1998; G. R. Hu, unpub. Ph.D. thesis, Nanjing Univ. 1998). The Palaeo- to Mesoproterozoic basement consists mainly of schists, granulitites and amphibolites. The schist is composed mainly of biotite, plagioclase and quartz, whereas granulitite consists mainly of quartz, plagioclase and biotite. Amphibole, plagioclase and quartz make up the amphibolite. G. R. Hu (unpub. Ph.D. thesis, Nanjing Univ., 1998) suggested that the protoliths of the schists and granulitites were of sedimentary origin (parametamorphic rocks), whereas the precursor to the amphibolites was basaltic (orthometamorphic rocks).

Both the Qianlishan porphyritic biotite granite and equigranular biotite granite show higher ε_{Nd} (T) values than Palaeoproterozoic parametamorphic rocks, but lower than orthometamorphic rocks at the age of intrusion (Fig. 9a). Their initial $^{87}Sr/^{86}Sr$ ratios are lower than those of Palaeoproterozoic parametamorphic rocks, but similar to those of orthometamorphic rocks at the age of intrusion (Fig. 9a). The calculated T_{DM} values of the porphyritic biotite granite range from 1949 to 2632 Ma (average 2307 Ma) (Table 4). The equigranular biotite granites have negative T_{DM} values due to the fractionation supported by high Sm/Nd ratios (0.23–0.35, Table 4). These may suggest that both the porphyritic biotite granite and equigranular biotite granite were derived by partial melting
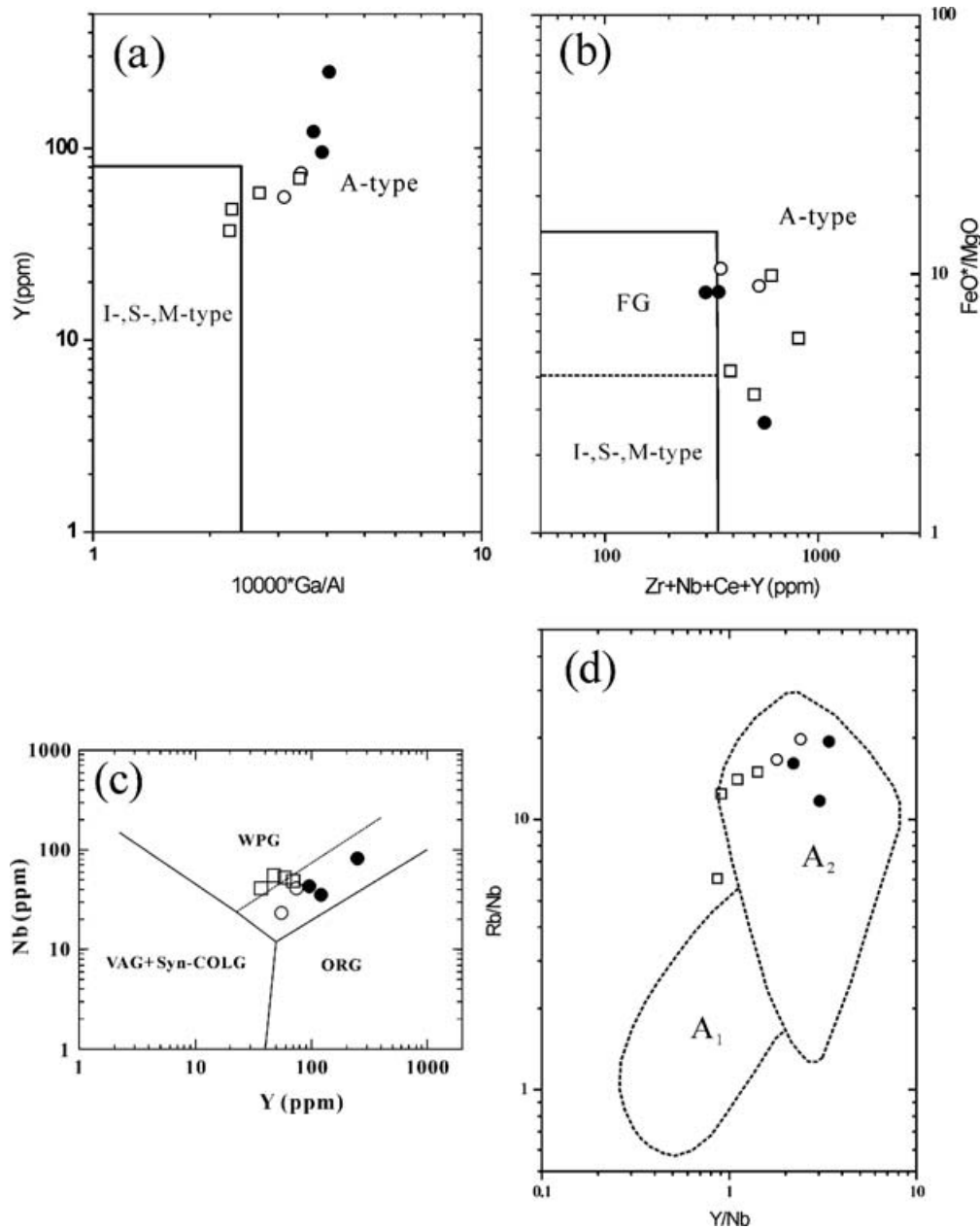
Figure 10. 10000*Ga/Al v. Y (a), Zr+Nb+Ce+Y v. FeO*/MgO (b) from Whalen, Currie & Chappell (1987), Y v. Nb (c) from Pearce, Harris & Tindle (1984) and Y/Nb v. Rb/Nb (d) from Eby (1992). WPG – within-plate granite, VAG – volcanic arc granite, Syn-COLG – syn-collision granite, ORG – ocean ridge granite, FG – fractionated granite. Symbols as in Figure 3.

of Palaeoproterozoic metamorphic rocks including both orthometamorphic and parametamorphic rocks at depth. The granite-porphyry dykes have T_{DM} values of 1284–1578 Ma (average 1434 Ma) (Table 4) and show higher ε_{Nd} (T) values than Mesoproterozoic parametamorphic rocks but lower than orthometamorphic rocks at the age of intrusion (Fig. 9a), whereas their initial $^{87}Sr/^{86}Sr$ ratios are lower than that of the Mesoproterozoic metamorphic rocks (Fig. 9a). Therefore we propose that the granite-porphyry dykes were derived from partial melting of Mesoproterozoic metamorphic rocks, including both orthometamorphic and parametamorphic rocks at depth, but we cannot

rule out the contributions from the underplating mafic magmas to the granite-porphyry dykes.

6.a.3. Elemental constraints

High and constant values of both K_2O and Na_2O (Table 4) may require the presence of a K-rich phase such as K-feldspar or biotite and Na-rich phase such as plagioclase in the source region. The Sr- and Ba-depleted nature of the granitic rocks (Fig. 8a) also indicates that plagioclase and K-feldspar were present in the sources. In addition, the granitic rocks have very high Rb concentrations (335–962 ppm, Table 4)

Figure 11. Rb v. Rb/Ba (a) and Rb/Sr (b) and La v. La/Sm (c) for the Qianlishan granitic rocks. Symbols as in Figure 3.

in both plagioclase ($K_{Rb} = 0.041$) and amphibole ($K_{Rb} = 0.014$) (Arth, 1976), the granitic rocks have very low Sr concentrations (10–102 ppm, Table 4) and show positive correlations between the Rb concentrations and Rb/Sr ratios (Fig. 11b), suggesting plagioclase instead of amphibole in the sources. The Y-undepleted nature (Fig. 8a) and flat heavy REE patterns (Fig. 7a, b) indicate that garnet was absent from the source regions during partial melting. The positive correlations between the La concentrations and La/Sm ratios for the granitic rocks (Fig. 11c) suggest that orthopyroxene and/or clinopyroxene are present in the source region. The element La has a similar degree of incompatibility to Sm in K-feldspar, plagioclase and quartz, but is much more incompatible than Sm in orthopyroxene and/or clinopyroxene (Mahood & Hildreth, 1983). The increase in the La/Sm ratios for the Qianlishan granitic rocks with increasing La (Fig. 11c) requires that the bulk partition coefficients for Sm exceed that of La, which therefore requires the presence of orthopyroxene and/or clinopyroxene in the sources. The relatively constant La/Sm ratios of the equigranular biotite granite (Fig. 11c) suggest that after partial melting, the magma most probably underwent subsequent fractionation of K-feldspar and plagioclase, a suggestion supported by the most significant negative Eu, Ba and Sr anomalies (Figs 7a, 8a). Furthermore, the feldspar separated from equigranular biotite granite also shows strong Eu depletion, further suggesting that the equigranular biotite granite crystallized from an evolved melt (Zhao et al. 2002). The low P and Ti contents (Fig. 8a) and high Sm/Nd ratios (0.23–0.35, Table 4) of the equigranular biotite granite suggest crystal fractionation of apatite, ilmenite/rutile and allanite, respectively. It is also quite possible that the equigranular biotite granitic magma was evolved from the slightly earlier porphyritic biotite granitic magma by these crystal fractionations (Figs 7a, 8a). However, their different Sr–Nd isotopic compositions (Fig. 9a) rule out this possibility.

In the binary system Ab–An, the initial melt of a given composition plagioclase is enriched in the Ab component relative to the bulk composition, and the melt becomes progressively more enriched in the An component with increasing temperature. Therefore, the low CaO contents and notable negative Eu anomalies (Fig. 7a) of the biotite granites suggest a lesser degree of partial melting for their origin. However, the granite-porphyry dykes have higher CaO contents and show less negative Eu anomalies (Fig. 7b) than the biotite granites, together with higher MgO, TiO$_2$ and V and lower SiO$_2$ contents (Fig. 12), suggesting a greater degree of partial melting than that of the biotite granites for their origin. All together, it is suggested that the effects of partial melting and source compositions mainly control the compositional variation of the biotite granites and granite-porphyry dykes.
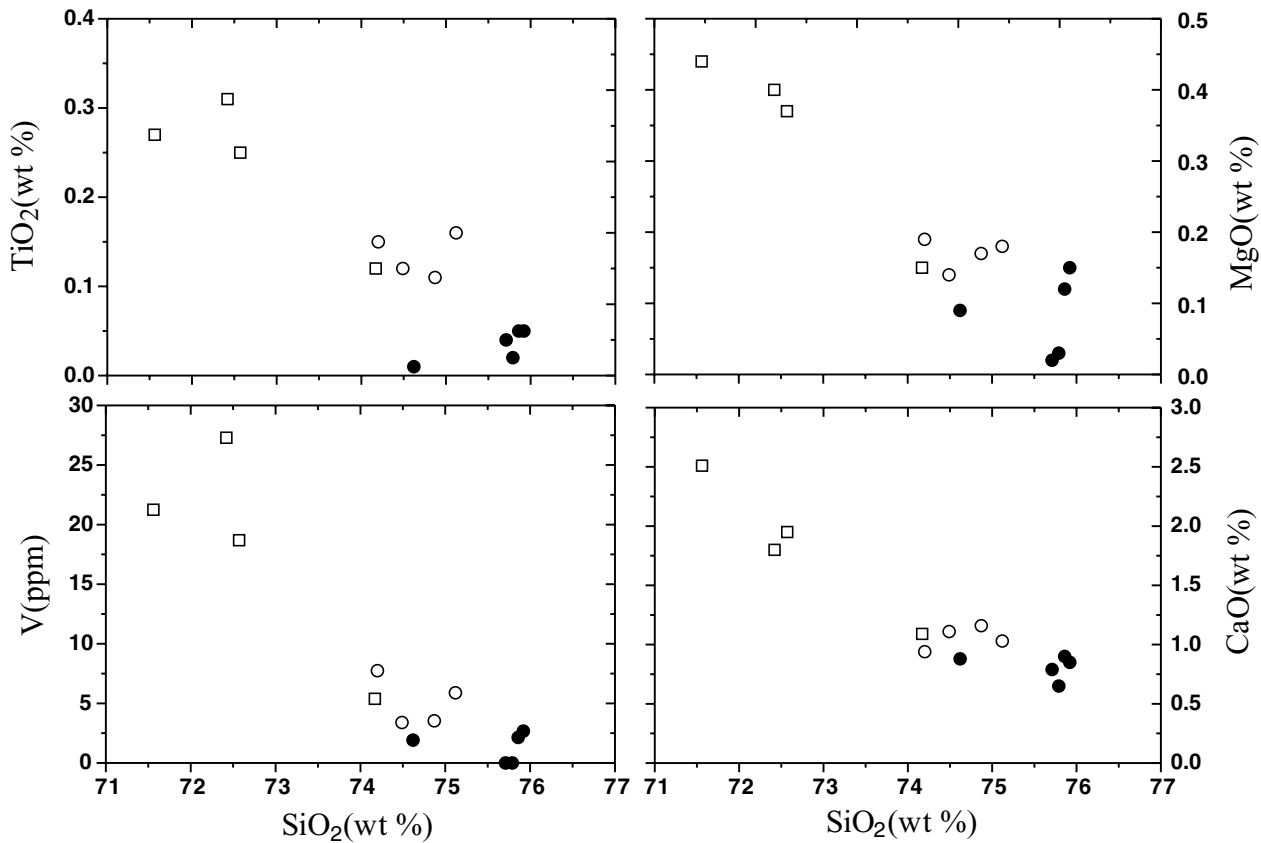
and show positive correlations between the Rb concentrations and Rb/Ba ratios (Fig. 11a), which further suggests K-feldspar, rather than biotite, as the main K-rich phase in the sources, considering that the element Rb is incompatible in K-feldspar (mineral/ acid-melt partition coefficient $K_{Rb} = 0.340$) but is compatible in biotite ($K_{Rb} = 2.240$), and that the element Ba is compatible in both K-feldspar ($K_{Ba} = 6.120$) and biotite ($K_{Ba} = 9.700$) (Arth, 1976). Similarly, because the element Sr is compatible in plagioclase ($K_{Sr} = 4.400$) but is incompatible in amphibole ($K_{Sr} = 0.022$) while the element Rb is incompatible

Figure 12. SiO_2 v. TiO_2, MgO, CaO and V for the Qianlishan granitic rocks. Symbols as in Figure 3.

6.a.4. Petrogenetic model

The characteristics of the Qianlishan granitic rocks mentioned above indicate that they were derived by partial melting of Palaeo- to Mesoproterozoic metamorphic rocks plus subsequent crystal fractionation for the equigranular biotite granite. The source rocks are suggested to contain K-feldspar (Kfs), plagioclase (Pl), quartz (Qtz) and orthopyroxene (Opx) ± clinopyroxene (Cpx). We prefer an alternative model for the source rocks of the Qianlishan A-type magma, that is, that Palaeo- to Mesoproterozoic metamorphic rocks in the lower crust were granulitized during the earlier thermal event. The probable reactions are:

$$Bt + Qtz + Pl = Opx \pm Cpx + Kfs + Melt$$
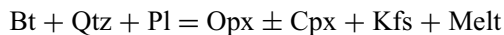
(Clemens & Wall, 1981; Landenberger & Collins, 1996) for parametamorphic rocks (schist and granulitite) and

$$Hbl + Qtz = Opx + Cpx + Pl + Melt$$
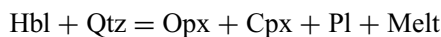
(Rushmer, 1991; Landenberger & Collins, 1996) for orthometamorphite (amphibolite). It is the continued supply of mantle-derived heat that is capable of elevating lower-crustal temperatures to above 850–900 °C, once the temperature buffering effect of these fluid-absent dehydration melting reactions is removed. In this way, anhydrous granulite-facies lower-crustal

assemblages (Kfs + Pl + Qtz + Opx ± Cpx) can be melted to produce the Qianlishan A-type magmas.

6.b. Origin of mafic dykes

The Qianlishan lamprophyre and neighbouring Guiyang mafic dykes are potassic in affinity. Nelson (1992) suggested that the potassic rock suite could be divided into an 'orogenic' sub-group, occurring in subduction-related tectonic settings, and an 'anorogenic' sub-group, occurring in stable continental settings. It has been proposed that most orogenic potassic magmas, such as Batu Tara (a potassic volcano in the eastern Sunda arc) and Roccamonfina (a volcano in the Italian potassic province), were derived from enriched mantle sources associated with the fluids or melts derived from a subducted slab (Peccerillo, 1990, 1999; Foley & Peccerillo, 1992; Rogers, 1992; Nelson, 1992; van Bergen *et al.* 1992). The Sr–Nd isotopic compositions of these orogenic potassic rocks plot along a mixing line between an upper mantle end-member with Sr and Nd isotopic compositions similar to mid-ocean ridge basalts, and an enriched mantle end-member with Sr and Nd isotopic compositions similar to those of oceanic sediments (Fig. 9b). The Qianlishan lamprophyre and Guiyang mafic dykes plot in the lower right quadrant and within the field of Batu Tara and
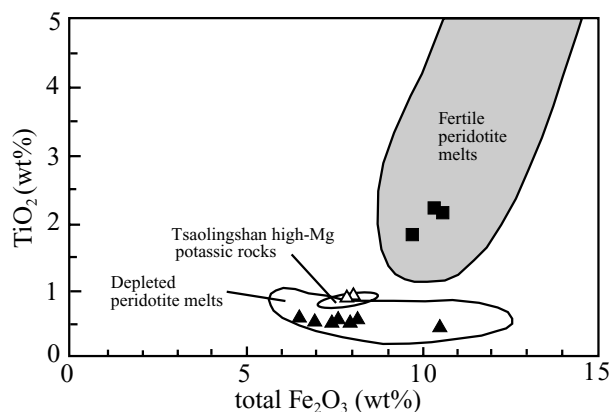
Figure 13. TiO$_2$ v. total Fe$_2$O$_3$ (wt %) for the Qianlishan mafic dykes compared with fields for some high-Mg potassic rocks (Chung *et al.* 2001) and experimental peridotite melts (Falloon *et al.* 1988). Symbols as in Figure 3. Original data for the Guiyang mafic dykes are from Wang *et al.* (2003).
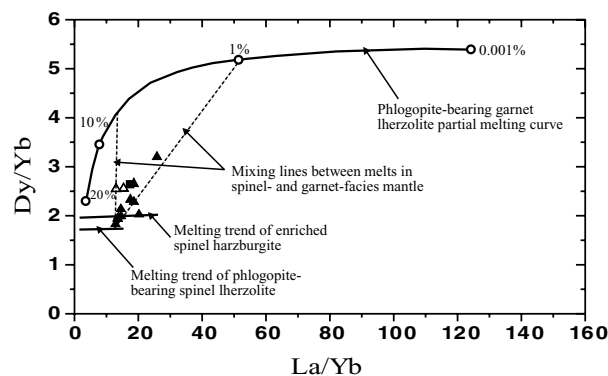

Figure 14. Variation of La/Yb and Dy/Yb for the Qianlishan and Guiyang mafic dykes with partial melting curves for phlogopite-bearing spinel and garnet lherzolites (after Miller *et al.* 1999) and enriched spinel harzburgite (after Xu *et al.* 2001). Source mineralogy is 55 % olivine, 25 % othopyroxene, 9 % clinopyroxene, 3 % spinel, 8 % phlogopite for phlogopite-bearing spinel lherzolite; 55 % olivine, 19 % othopyroxene, 7 % clinopyroxene, 11 % garnet, 8 % phlogopite for phlogopite-bearing garnet lherzolite; 70 % olivine, 23 % orthopyroxene, 5 % clinopyroxene, 2 % spinel for enriched spinel harzburgite. Symbols as in Figure 3. Original data for the Guiyang mafic dykes are from Wang *et al.* (2003).

Roccamonfina potassic rocks in the Sr–Nd isotope diagram (Fig. 9b). Together with their high contents of LREE and LILE (Table 4), we suggest that these dykes may also have been derived from an enriched mantle source associated with the fluids or melts derived from a subducted slab.

The Qianlishan lamprophyre dykes have low TiO$_2$ contents and plot in the field defined by experimental melts of depleted peridotite (Falloon *et al.* 1988) (Fig. 13), similar to the Guiyang mafic dykes. Together with their high compatible element contents, we suggest that these mafic dykes were derived from a refractory lithospheric mantle. The Qianlishan lamprophyres show notable negative Ba, Nb-Ta, Sr and Ti anomalies, but with Cs, Rb, Th and U strongly enriched (Fig. 8a), which is very similar to the Tsaolingshan (Taiwan) high-Mg potassic rocks that have been proposed as deriving from a phlogopite-bearing harzburgitic source in the lithospheric mantle (Chung *et al.* 2001). The Qianlishan lamprophyres have very high Rb contents (2756–3856 ppm) and extraordinarily high Rb/Sr (1.14) and low Ba/Rb (1.06–1.31) ratios (Table 4), consistent with the Tsaolingshan high-Mg potassic rocks (Rb = 1025–2114 ppm, Rb/Sr = 1.52–3.16, Ba/Rb = 0.47–1.00; Chung *et al.* 2001), which is owing to a slab-derived fluid enrichment in the mantle source region (Chung *et al.* 2001). The Nb/U (3.2–15.1) and Ce/Pb (3.4–15.6) ratios for the Qianlishan lamprophyre and Guiyang mafic dykes (Table 4) are lower than those of MORB and OIB (47 and 27, respectively: Hofmann *et al.* 1986), indicating the involvement of crustal components in their sources. The depletion of HFSE relative to LILE (e.g. Ta, Nb and Hf relative to U, La and Sm, respectively, Fig. 8b) is considered to be indicative of subduction processes (e.g. Thirlwall *et al.* 1994). All together, we propose a subduction-modified refractory lithospheric mantle

source for the origin the Qianlishan lamprophyre and Guiyang mafic dykes.

The Qianlishan diabases have high TiO$_2$ contents and plot in the field defined by experimental melts of fertile peridotite (Falloon *et al.* 1988) (Fig. 13), together with the positive ε_{Nd} (T) value (Fig. 9b), suggesting that they were most probably derived from fertile asthenophere. However, these diabases are also enriched in LREE (Fig. 7c) and LILE and relatively depleted in HFSE (Fig. 8b), implying that the asthenospheric mantle was also affected by the subduction processes. This is further supported by relatively high initial ^{87}Sr/^{86}Sr ratio of the diabase (Fig. 9b).

The high K$_2$O contents in mafic dykes require a potassic phase in the source region. Melts in equilibrium with phlogopite are expected to have significantly higher Rb/Sr (> 0.1) and lower Ba/Rb (< 20) ratios than those (Rb/Sr < 0.06 and Ba/Rb > 20, respectively) formed from amphibole-bearing mantle sources (Furman & Graham, 1999). The Qianlishan and Guiyang mafic dykes have high Rb/Sr (0.27–1.14) and low Ba/Rb (1.06–8.99) ratios (Table 4), suggesting that the mafic magmas formed through melting of a phlogopite-bearing mantle source. There is little change in La/Yb ratios, and Dy/Yb ratios remain almost constant during melting in the spinel stability field, whereas melting in the garnet stability field produces large changes in Dy/Yb and La/Yb ratios (Fig. 14). Figure 14 shows that the Qianlishan and Guiyang mafic dykes were most probably derived by partial melting of spinel-facies mantle plus a small portion of partial melt from garnet-facies mantle (about 1–8 % of melting). It is generally considered that the transition belt of
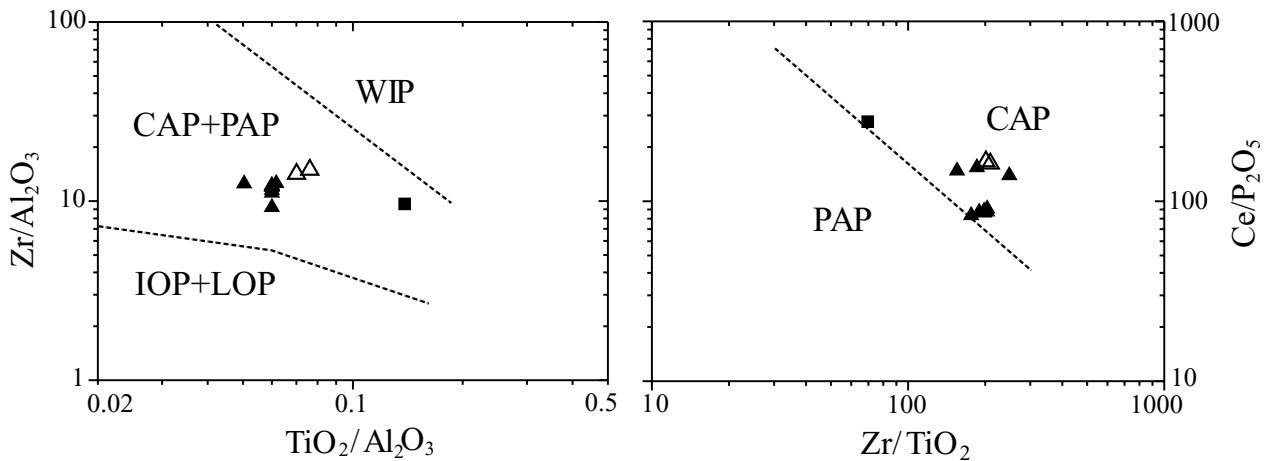
Figure 15. TiO_2/Al_2O_3 v. Zr/Al_2O_3 and Zr/TiO_2 v. Ce/P_2O_5 diagrams from Muller, Rock & Groves (1992). WIP – Within-plate potassic rocks, CAP – continental arc potassic rocks, PAP – post-collisional arc potassic rocks, IOP – initial oceanic arc potassic rocks, LOP – late oceanic arc potassic rocks. Symbols as in Figure 3. The original data of the Guiyang mafic dykes from Wang *et al.* (2003).

spinel-garnet facies mantle is at a depth of 60–80 km. It follows that partial melting took place at a shallower level (< 80 km) in the mantle source for these mafic magmas.

6.c. Tectonic environment

It has been recognized that A-type magmas are formed in a variety of extensional regimes, from continental back-arc extension to post-collisional extension and within-plate settings (e.g. Eby, 1992; Whalen *et al.* 1996; Förster, Tischendorf & Trumbull, 1997). Eby (1992) suggested that the A_1 group seemed to be restricted to hotspots, plumes and continental rift zones located in anorogenic settings. However, the A_2 group granitoids are emplaced in a variety of tectonic settings and there seems to be no way to distinguish chemically between these tectonic possibilities (Eby, 1992). As mentioned above, the Qianlishan granitic rocks belong to the A_2 group. We can thus rule out an origin related to a hot spot, plume or continental rift zone located in anorogenic settings.

Potassic (shoshonitic) rocks typically occur in destructive plate margin settings, as the arc matures, and are generally younger than the tholeiitic and calc-alkaline rocks (Morrison, 1980). It has been proposed that such potassic rocks also occur in extensional environments such as post-collisional and continental rift tectonic settings (Muller, Rock & Groves, 1992; Turner, Arnaud & Liu, 1996; Eklund *et al.* 1998; Rogers, James & Kelley, 1998; Liégeois *et al.* 1998; Jiang *et al.* 2002). Muller, Rock & Groves (1992) conducted a pilot study on geochemical discrimination for potassic rocks ($SiO_2 = 41.4$–62.1 wt % and $K_2O = 0.4$–8.4 wt %) formed in different tectonic settings. The Qianlishan and Guiyang mafic dyke data plot in the continental arc, rather than within-plate and post-collisional arc fields in these discrimination diagrams

(Fig. 15). Such a setting is characterized by relatively flat subduction angles and broad Benioff zones (Muller, Rock & Groves, 1992).

Integrating the information from the Qianlishan A-type granitic rocks and coeval potassic dykes, only a continental back-arc extensional setting could be suggested for both the granitic rocks and mafic dykes. Contemporaneous (158–135 Ma) bimodal magmatism within the Shi-Hang zone also occurs further to the northeast of Qianlishan in the Xiangshan area, Jiangxi province (Fig. 1) (Jiang *et al.* 2005). More recently, Jiang *et al.* (2005) studied the Xiangshan volcanic complex and its quenched mafic enclaves, and concluded that the Xiangshan volcanic complex also shows an A-type affinity, and that its quenched mafic enclaves are high-Mg potassic rocks. This also suggests a back-arc extensional setting, related to subduction of the Palaeo-Pacific plate. Therefore, it is most likely that the Shi-Hang zone is part of a back-arc extensional zone.

7. Conclusions

The Late Jurassic Qianlishan granitic rocks show A_2 subtype affinity, most probably derived by partial melting of Palaeo- to Mesoproterozoic metamorphic basement in the lower crust. These metamorphic rocks include both orthometamorphic and parametamorphic rocks that had been granulitized during an earlier (180–160 Ma) thermal event. The coeval Qianlishan lamprophyre and Guiyang mafic dykes are high-Mg potassic rocks, suggesting derivation from a subduction-modified refractory lithospheric mantle (phlogopite-bearing harzburgite or lherzolite) at the depth of < 80 km. The coeval Qianlishan diabases are alkaline and have high TiO_2 and total Fe_2O_3 contents, suggesting derivation from fertile asthenospheric mantle (phlogopite-bearing lherzolite) at the depth of < 80 km.

Detailed petrological and geochemical data for the Qianlishan granitic rocks and mafic dykes imply that they were generated in a back-arc extensional regime. This suggests that the late Mesozoic volcanic-intrusive complex belt in Southeast China was related to subduction of the Palaeo-Pacific plate. Between 180 and 160 Ma, Southeast China was a continental arc, forming the 180–160 Ma plutons, and the lower-crust was granulitized. Since 160 Ma the northwestern belt has been in a back-arc extensional setting as a consequence of slab roll-back, resulting in the lithosphere thinning and an influx of asthenophere. The upwelling asthenosphere, on the one hand, induced the local lithospheric mantle to melt partially, forming high-Mg potassic magmas, and on the other hand it underwent decompression melting itself to form alkaline diabase magma. Pulsatory injection of such high-temperature magmas into the granulitized crustal source region induced them to melt partially and generate the A-type magmas of the Qianlishan granitic rocks.

References

ARTH, J. G. 1976. Behavior of trace elements during magmatic processes – a summary of theoretical models and their applications. *Journal of Research of the US Geological Survey* **4**, 41–7.

BLOOMER, S. H. & HAWKINS, J. M. 1987. Petrology and geochemistry of boninite series volcanic rocks from the Mariana Trench. *Contributions to Mineralogy and Petrology* **97**, 361–77.

CHAPPELL, B. W. & WHITE, A. J. K. 1974. Two contrasting granite types. *Pacific Geology* **8**, 173–4.

CHARVET, J., LAPIERRE, H. & YU, Y. 1994. Geodynamic significance of the Mesozoic volcanism of southeastern China. *Journal of Southeast Asian Earth Sciences* **68**, 387–96.

CHUNG, S. L., WANG, K. L., CRAWFORD, A. J., KAMENETSKY, V. S., CHEN, C. H., LAN, C. Y. & CHEN, C. H. 2001. High-Mg potassic rocks from Taiwan: implications for the genesis of orogenic potassic lavas. *Lithos* **59**, 153–70.

CLEMENS, J. D. & WALL, V. J. 1981. Crystallisation and origin of some peraluminous (S-type) granitic magmas. *Canadian Mineralogist* **19**, 111–32.

COLLINS, W. J., BEAMS, S. D. & WHITE, A. J. R. 1982. Nature and origin of A-type granites with particular reference to southeastern Australia. *Contributions to Mineralogy and Petrology* **80**, 189–200.

CREASER, R. A., PRICE, R. C. & WORMALD, R. J. 1991. A-type granites revisited: assessment of a residual source model. *Geology* **19**, 163–6.

DEER, W. A., HOWIE, R. A. & ZUSSMAN, J. 1992. *An Introduction to the Rock-forming Minerals*, 2nd ed. Harlow: Longman Group UK, 232 pp.

EBY, G. N. 1992. Chemical subdivision of the A-type granitoids: petrogenetic and tectonic implications. *Geology* **20**, 641–4.

EKLUND, O., KONOPELKO, D., RUTANEN, H., FRÖJDÖ, S. & SHEBANOV, A. D. 1998. 1.8 Ga Svecofennian post-collisional shoshonitic magmatism in the Fennoscandian shield. *Lithos* **45**, 87–108.

FALLOON, T. J., GREEN, D. H., HATTON, C. J. & HARRIS, K. L. 1988. Anhydrous partial melting of a fertile and depleted peridotite from 2 to 30 kb and application to basalt petrogenesis. *Journal of Petrology* **29**, 1257–82.

FOLEY, S. & PECCERILLO, A. 1992. Potassic and ultrapotassic magmas and their origin. *Lithos* **28**, 181–6.

FÖRSTER, H. J., TISCHENDORF, G. & TRUMBULL, R. B. 1997. An evaluation of the Rb vs. (Y+Nb) discrimination diagram to infer tectonic setting of silicic igneous rocks. *Lithos* **40**, 261–93.

FOSTER, M. D. 1960. Interpretation of the composition of trioctahedral mica. *U.S. Geological Survey Professional Paper* **354-B**, 11–48.

FURMAN, T. & GRAHAM, D. 1999. Erosion of lithospheric mantle beneath the East African Rift system: geochemical evidence from the Kivu volcanic province. *Lithos* **48**, 237–62.

GILDER, S. A., KELLER, G. R., LUO, M. & GOODELL, P. C. 1991. Timing and spatial distribution of rifting in China. *Tectonophysics* **197**, 225–43.

GILDER, S. A., GILL, J., COE, R. S., ZHAO, X., LIU, Z., WANG, G., YUAN, K., LIU, W., KUANG, G. & WU, H. 1996. Isotopic and paleomagnetic constraints on the Mesozoic tectonic evolution of south China. *Journal of Geophysical Research* **101**, 16137–54.

HICKEY, R. L. & FREY, F. A. 1982. Geochemical characteristics of boninite series volcanics: implications for their source. *Geochimica et Cosmochimica Acta* **46**, 2099–115.

HOFMANN, A., JOCHUM, K., SEUFERT, M. & WHITE, M. 1986. Nb and Pb in oceanic basalts: new constraints on mantle evolution. *Earth and Planetary Science Letters* **33**, 33–45.

JIANG, Y. H., JIANG, S. Y., LING, H. F., ZHOU, X. R., RUI, X. J. & YANG, W. Z. 2002. Petrology and geochemistry of shoshonitic plutons from the western Kunlun orogenic belt, northwestern Xinjiang, China: implications for granitoid geneses. *Lithos* **63**, 165–87.

JIANG, Y. H., LING, H. F., JIANG, S. Y., FAN, H. H., SHEN, W. Z. & NI, P. 2005. Petrogenesis of Late Jurassic peraluminous volcanic complex and its high-Mg, potassic, quenched enclaves at Xiangshan, Southeast China. *Journal of Petrology* **46**, 1121–54.

LANDENBERGER, B. & COLLINS, W. J. 1996. Derivation of A-type granites from a dehydrated charnockitic lower crust: evidence from the Chaelundi complex, eastern Australia. *Journal of Petrology* **37**, 145–70.

LAPIERRE, H., JAHN, B. M. & CHARVET, J. 1997. Mesozoic magmatism in Zhejiang Province and its relation with the tectonic activities in SE China. *Tectonophysics* **274**, 321–38.

LI, X. H. 1999. Magmatism and lithosphere extension of Cretaceous in south China. In *Natural Resources, Environment and Sustainable Development* (ed. the Institute of Geochemistry Academia Sinica), pp. 264–75. Beijing: Since Press.

LI, X. H., WANG, Y. X., ZHAO, Z. H., CHEN, D. F. & ZHANG, H. 1998. SHRIMP U–Pb zircon geochronology for amphibolite from the precambrian basement in SW Zhejiang and NW Fujian Province. *Geochimica* **27**, 327–34 (in Chinese with English abstract).

LI, X. H., LIU, D. Y., SUN, M., LI, W. X., LIANG, X. R. & LIU, Y. 2004. Precise Sm–Nd and U–Pb isotopic dating of the supergiant Shizhuyuan polymetallic deposit and its host granite, SE China. *Geological Magazine* **141**, 225–31.

LIAO, Q. A., WANG, J. M., XUE, C. S. & LI, C. N. 1999. Characteristics of basalts in Cretaceous basin and their relations with the basin's evolution at Guangfeng, Jiangxi province. *Acta Petrologica Sinica* **15**, 116–23 (in Chinese with English abstract).

LIÉGEOIS, J. P., NAVEZ, J., HERTOGEN, J. & BLACK, R. 1998. Contrasting origin of post-collisional high-K calc-alkaline and shoshonitic versus alkaline and peralkaline granitoids. The use of sliding normalization. *Lithos* **45**, 1–28.

LIU, Y. M., DAI, T. M., LU, H. Z., XU, Y., WANG, C. L. & KANG, W. Q. 1997. ^{40}Ar–^{39}Ar and Sm–Nd dating of Qianlishan granites, SE China. *Science in China (Series D)* **27**, 425–30.

MAHOOD, G. & HILDRETH, W. 1983. Large partition coefficients for trace elements in high-silica rhyolites. *Geochimica et Cosmochimica Acta* **47**, 11–30.

MAO, J. W., LI, H. Y., SONG, X. X., RUI, B., XU, Y., WANG, D. H., LAN, X. M. & ZHANG, K. J. 1998. *Geology and geochemistry of the Shizhuyuan W-Sn-Mo-Bi polymetallic deposit, Hunan, China*. Beijing: Geological Publishing House, 215 pp.

MARTIN, H., BONIN, B. & CAPDEVILA, R. 1994. The Kuiqi peralkaline granitic complex (SE China): petrology and geochemistry. *Journal of Petrology* **35**, 983–1015.

MILLER, C., SCHUSTER, R., KLÖTZLI, U., FRANK, W. & PURTSCHELLER, F. 1999. Post-collisional potassic and ultrapotassic magmatism in SW Tibet: geochemical and Sr-Nd-Pb-O isotopic constraints for mantle source characteristics and petrogenesis. *Journal of Petrology* **40**, 1399–424.

MORRISON, G. W. 1980. Characteristics and tectonic setting of the shoshonite rock association. *Lithos* **13**, 97–108.

MULLER, D., ROCK, N. M. S. & GROVES, D. I. 1992. Geochemical discrimination between shoshonitic and potassic volcanic rocks in different tectonic settings: a pilot study. *Mineralogy and Petrology* **46**, 259–89.

NELSON, D. R. 1992. Isotopic characteristics of potassic rocks: evidence for the involvement of subducted sediments in magma genesis. *Lithos* **28**, 403–20.

PEARCE, J. A., HARRIS, N. B. W. & TINDLE, A. G. 1984. Trace element discrimination diagrams for the tectonic interpretation of granitic rocks. *Journal of Petrology* **25**, 956–83.

PECCERILLO, A. 1990. On the origin of the Italian potassic magma—comments. *Chemical Geology* **85**, 183–96.

PECCERILLO, A. 1999. Multiple mantle metasomatism in central–southern Italy: geochemical effects, timing and geodynamic implications. *Geology* **27**, 315–18.

PITCHER, W. S. 1983. Granite type and tectonic environment. In *Mountain Building Processes* (ed. K. Hsu), pp. 19–40. London: Academic Press.

ROGERS, N. W. 1992. Potassic magmatism as a key to trace-element enrichment processes in the uppper mantle. *Journal of Volcanology and Geothermal Research* **50**, 85–99.

ROGERS, N. W., JAMES, D. & KELLEY, S. P. 1998. The generation of potassic lava from the eastern Virunga province, Rwanda. *Journal of Petrology* **39**, 1223–47.

RUSHMER, T. 1991. Partial melting of two amphibolites: contrasting experimental results under fluid-absent conditions. *Contributions to Mineralogy and Petrology* **107**, 41–59.

SHEN, W. Z., WANG, D. Z., XIE, Y. L. & LIU, C. S. 1995. Geochemical characteristics and material sources of Qianlishan composite granites, Hunan province. *Acta Petrologica et Mineralogica* **14**, 193–202 (in Chinese with English abstract).

STRECKEISEN, A. 1976. To each plutonic rock its proper name. *Earth Science Reviews* **12**, 1–33.

THIRLWALL, M. F., SMITH, T. E., GRAHAM, A. M., THEODOROU, N., HOLLINGS, P., DAVIDSON, J. P. & ARCULUS, R. J. 1994. High field strength element anomalies in arc lavas: source or process? *Journal of Petrology* **35**, 819–38.

TURNER, S., ARNAUD, N. & LIU, J. 1996. Post-collision shoshonitic volcanism on the Tibetan plateau: Implications for convective thinning of the lithosphere and the source of ocean island basalts. *Journal of Petrology* **37**, 45–71.

TURNER, S. P., FODEN, J. D. & MORRISON, R. S. 1992. Derivation of some A-type magmas by fractionation of basaltic magma: an example from the Pasthaway Ridge, south Australia. *Lithos* **28**, 151–79.

VAN BERGEN, M. J., VROON, P. Z., VAREKAMP, J. C. & POORTER, R. P. E. 1992. The origin of the potassic rock suite from Batu Tara volcano (East Sunda Arc, Indonesia). *Lithos* **28**, 261–82.

WANG, C. L., LUO, S., XU, Y., SUN, Y., XIE, C., ZHANG, Z., XU, W. & REN, X. 1987. *Geology of the Shizhuyuan Tungsten-Polymetallic Deposit*. Beijing: Geological Publishing House, 173 pp.

WANG, Y. J., FAN, W. M., GUO, F., PENG, T. P. & LI, C. W. 2003. Geochemistry of Mesozoic mafic rocks adjacent to the Chenzhou-Linwu fault, South China: implications for the lithospheric boundary between the Yangtze and Cathaysia blocks. *International Geology Review* **45**, 263–86.

WHALEN, J. B., CURRIE, K. L. & CHAPPELL, B. W. 1987. A-type granites: geochemical characteristics, discrimination and petrogenesis. *Contributions to Mineralogy and Petrology* **95**, 407–19.

WHALEN, J. B., JENNER, G. A., LONGSTAFFE, F. J., ROBERT, F. & GARIEPY, C. 1996. Geochemical and isotopic (O, Nd, Pb and Sr) constraints on A-type granite petrogenesis based on the Topsails igneous suite, Newfoundland Appalachians. *Journal of Petrology* **37**, 1463–89.

WRIGHT, J. B. 1969. A simple alkalinity ratio and its application to questions of non-orogenic granite genesis. *Geological Magazine* **106**, 370–84.

XU, Y. G., MENZIES, M. A., THIRLWALL, M. F. & XIE, G. H. 2001. Exotic lithosphere mantle beneath the western Yangtze craton: petrogenetic links to Tibet using highly magnesian ultrapotassic rocks. *Geology* **29**, 863–6.

YU, D. G., YE, F. W. & WANG, Y. 2001. Active succession establishment and its geological implication of Early Cretaceous intrusive-volcanic complexes in Guangfeng basin, Jiangxi province. *Geotectonic et Metallogenia* **25**, 271–6 (in Chinese with English abstract).

YUAN, Z. X., WU, L. S., ZHANG, Z. Q. & YE, X. J. 1991. Study on Sm-Nd and Rb-Sr isotopic age of the Mayuan Group

in Northern Fujian. *Acta Petrologica et Mineralogica* **10**, 127–32 (in Chinese with English abstract).

ZHANG, Z. Q., LIU, D. Y. & FU, G. M. 1994. *Study of isotopic geochronology of metamorphic rock in the northern Qinling*. Beijing: Geological Publishing House, 158 pp.

ZHAO, Z. H., BAO, Z. W., ZHANG, B. Y. & XIONG, X. L. 2001. Crust-mantle interaction and its contribution to the Shizhuyuan superlarge tungsten polymetallic mineralization. *Science in China (Series D)* **44**, 266–76 (in Chinese).

ZHAO, Z. H., XIONG, X. L., HAN, X. D., WANG, Y. X., WANG, Q., BAO, Z. W. & JAHN, B. 2002. Controls on the REE

tetrad effect in granites: Evidence from the Qianlishan and Baerzhe granites, China. *Geochemical Journal* **36**, 527–43.

ZHENG, Q. R. 1983. Calculation of the Fe^{3+} and Fe^{2+} contents in silicate and Ti–Fe oxide minerals from epma data. *Acta Mineralogica Sinica* **3**, 55–62.

ZHOU, X. M. & LI, W. X. 2000. Origin of late Mesozoic igneous rocks in southeastern China: implications for lithosphere subduction and underplating of mafic magmas. *Tectonophysics* **326**, 269–87.

ZHOU, X. R. & WU, K. L. 1994. *I- and A-type composite granite in Zhangzhou*. Beijing: Science Press, 148 pp.